

AlPO₄ in Silica Glass Optical Fibers: Deduction of Additional Material Properties

(Invited Paper)

Volume 11, Number 5, October 2019

Nanjie Yu, *Student Member, IEEE*

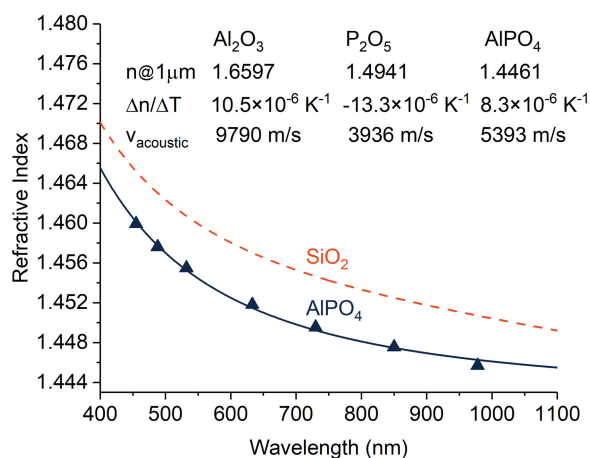
Thomas W. Hawkins

Thao-Vien Bui

Maxime Cavillon

John Ballato, *Fellow, IEEE*





Peter D. Dragic, *Member, IEEE*



DOI: 10.1109/JPHOT.2019.2941487

AlPO₄ in Silica Glass Optical Fibers: Deduction of Additional Material Properties

(Invited Paper)

Nanjie Yu ¹, *Student Member, IEEE*, Thomas W. Hawkins,²
Thao-Vien Bui ¹, Maxime Cavillon ²,
John Ballato ², *Fellow, IEEE*, and Peter D. Dragic,¹ *Member, IEEE*

¹Department of Electrical and Computer Engineering, University of Illinois at Urbana-Champaign, Urbana, IL 61801 USA

²Center for Optical Materials Science and Engineering Technologies and the Department of Materials Science and Engineering, Clemson University, Anderson, SC 29625 USA

DOI:10.1109/JPHOT.2019.2941487

This work is licensed under a Creative Commons Attribution 4.0 License. For more information, see <https://creativecommons.org/licenses/by/4.0/>

Manuscript received August 5, 2019; revised September 6, 2019; accepted September 11, 2019. Date of publication September 16, 2019; date of current version October 4, 2019. This work was supported by the US Department of Defense Joint Directed Energy Transition Office (DE-JTO) under Contracts W911NF-05-1-0517, FA9550-07-1-0566, W911NF-12-1-0602, FA9451-15-D-0009/0001 and 0002, and N00014-17-1-2546. The work of J. Ballato, T. W. Hawkins, and M. Cavillon was supported by the J. E. Serrine Foundation. Corresponding author: Nanjie Yu (e-mail: nanjey2@illinois.edu).

Abstract: A silica clad optical fiber with a core comprised of SiO₂, P₂O₅, Al₂O₃, and AlPO₄ is analyzed in order to determine the impact of AlPO₄ when added to silica. A chromatic dispersion curve is presented, from which the nonlinear refractive index is estimated to be similar to that of silica. When doped into SiO₂, AlPO₄ decreases the thermo-optic coefficient (slightly), decreases the acoustic velocity, broadens the Brillouin spectral width through increased viscoelastic damping, and reduces the strength of the dependence of Brillouin frequency on temperature. Findings herein indicate that AlPO₄ has a near-zero value of p_{12} . It also is found that the fiber does not have complete AlPO₄ formation, with some P₂O₅ formation in Al₂O₃-rich regions of the fiber. Given the relevance of AlPO₄ to high power active fiber technology, the presented data can be used for designing fibers with enhanced performance characteristics, such as those with elevated threshold for the onset of stimulated Brillouin scattering.

Index Terms: Fiber optics, fiber lasers, fiber nonlinear optics, optical fiber testing, optical materials, glass, aluminum, phosphorus.

1. Introduction

High power fiber lasers have matured considerably over the past two decades, and a number of excellent reviews devoted to the topic can be found in the literature [1]–[9]. As is outlined in these reviews, power scaling in fiber lasers, specifically single mode fiber lasers, is not endless, but, rather, can be limited by one or more of several nonlinear phenomena. The dominant nonlinear process depends strongly on the requirements of the fiber laser (e.g., narrow linewidth, high peak power, multi-wavelength, etc.). As such, power scaling efforts have largely focused on enhancing the mode size in the fiber in order to decrease the light intensity. In conventional step index fibers, this could entail decreasing the numerical aperture (NA) and increasing the core diameter of a

silica clad fiber [10], although such fibers can become difficult to fabricate. Reduction of the NA also can be accomplished through pedestal fiber designs, where the fiber possesses a high-index inner cladding surrounding the core [11]. Alternatively, the fiber may be microstructured to achieve effective single mode operation, with an excellent review that can be found in [12].

Focusing now on refractive index (or NA) control, it is well known that both Al₂O₃ and P₂O₅ raise the refractive index when added to silica. The peculiarity of these dopants is when they appear together, as they can form the ≡Al-O-P≡ structure (AlPO₄), which not only preserves the tetrahedral network [13], but also reduces the refractive index when added to silica [14]. In this work, these three oxide compounds, Al₂O₃, P₂O₅, and AlPO₄, are treated as three distinct materials, each bringing its own unique physical characteristics to the glass. While reference may be made herein to “Al” or “P” it is important to state that both are present as oxides within the glass, and therefore that this is not meant to imply their elemental speciation. Instead, this nomenclature serves as a convenient accounting method for Al and P, as the relative distributions of each of Al₂O₃, P₂O₅, and AlPO₄ are determined. As an illustrative example, the ratio “Al/P” is the ratio of total number of Al’s in both the Al₂O₃ and AlPO₄ phases to the total number of P’s in both P₂O₅ and AlPO₄ at some point on the fiber radial cross section.

Much work has been done to characterize the impact of AlPO₄ on the refractive index [15], rare earth spectroscopy, and glass itself, when added to silica. For instance, Likhachev, *et al.* [16] showed that P-rich Er-doped fibers (where the molar content of P is greater than that of Al) have emission spectra resembling phosphosilicate glasses. Jetschke, *et al.* [17] showed that with proper composition such a system can be effective in suppressing photodarkening [18], something corroborated by Deschamps, *et al.* [19] in P₂O₅-rich glasses possessing AlPO₄. More recently, Kuhn, *et al.* [20] showed that even when the ratio Al/P is approximately unity, there may be incomplete formation of AlPO₄ leaving some residual in P₂O₅ and Al₂O₃ phases, respectively, having a significant impact on the core refractive index.

While substantial effort has been undertaken in developing fibers along the AlPO₄ join, there still are several fundamental unknowns regarding this material. The purpose of this paper is therefore to further elucidate and enumerate the influence of AlPO₄ when doped into silica. To achieve this goal, a fiber with a core possessing SiO₂, P₂O₅, Al₂O₃, and AlPO₄ fabricated using the conventional modified chemical vapor deposition (MCVD) method, is analyzed. The core of this fiber has a varying ratio of Al/P across the radial dimension. Multi-wavelength refractive index measurements are performed in order to estimate the chromatic dispersion, and, from this, the nonlinear refractive index (n_2) is estimated and found to be nearly identical to that of silica. Brillouin spectroscopy also was performed on the fiber in order to determine the effect of AlPO₄ on the acoustic velocity, the Brillouin spectral width, and Brillouin gain coefficient. Furthermore, the findings here support that AlPO₄ formation in optical fiber need not be complete [20], but it is suggested that this likely is a strong function of fabrication history.

2. Fiber Fabrication

For this work, a preform was fabricated by means of MCVD method. Using a silica substrate tube (Heraeus Tenevo F300) with an inner diameter (ID) of 19 mm and outer diameter (OD) of 25 mm, a core layer of P₂O₅ was deposited on the inside of the tube. Once deposited, the substrate tube was removed from the lathe and prepped for solution doping. A solution of deionized water and aluminum chloride (AlCl₃; 99.999% purity, Alfa Aesar) at a ratio of 125 ml water and 150 grams AlCl₃ was mixed until it was fully dissolved in the water. The solution was pumped into the vertically mounted substrate tube and held for approximately 1 hour. The solution was then pumped out, and the tube interior was dried under nitrogen for an hour. After drying, the tube was remounted onto the lathe and fully consolidated into a rod with an approximate OD of 16 mm.

Once fully consolidated into a rod, the preform was drawn into fiber using a custom optical fiber draw tower (Heathway, Inc) at a temperature of approximately 2000 °C. The desired fiber OD was 95 μm in order to achieve a near-single-mode operation. A UV curable acrylate coating (Desolite 3471-3-14) was applied during the draw process to the exterior of the fiber. The coated fiber was

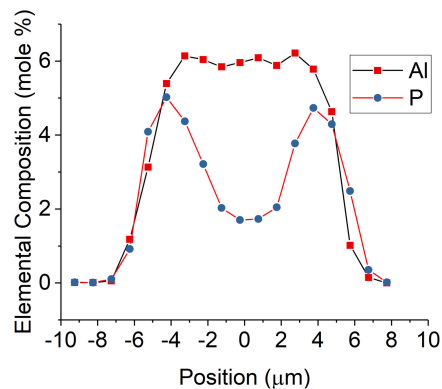


Fig. 1. Compositional profile measured via WDX for the fiber of the present study. (For visual clarity, SiO₂ concentrations are not shown here).

collected onto a standard 150 mm OD take-up spool and Approximately 50 m of fiber length was collected. The compositional profile was measured using wavelength dispersive X-ray analysis (WDX, Geller MicroAnalytical Laboratory, Inc.) with the results being provided in Fig. 1.

3. Experimental Details

With the goal of determining the influence of AlPO₄ as a dopant in silica, measurements are made to enumerate several physical characteristics of the fiber. These measurements have become a fairly standard set of tools used by these authors in the characterization of other optical fibers. Therefore, in order to spare the reader from verbosity, these methods are only briefly summarized below, and presented alongside a few relevant references should more details be desired.

3.1 Refractive Index

The refractive index profiles (RIPs) were measured using a form of spatially resolved Fourier Transform spectroscopy [21]. In order to determine the chromatic dispersion characteristics of the fiber, the refractive index differences (relative to silica) along two perpendicular directions in the fiber cross section were measured at seven wavelengths: 455 nm, 488 nm, 532 nm, 633 nm, 730 nm, 850 nm, and 978 nm. The spatial resolution in all cases was approximately 150 nm. As will be discussed, this measurement enabled the determination of the chromatic dispersion curve (hence Sellmeier coefficients) for the AlPO₄ dopant, along with an estimation of its nonlinear refractive index, n_2 .

3.2 Thermo-Optic Coefficient

To measure the thermo-optic response of the fiber, a ring laser cavity was utilized, with a segment of test fiber forming part of the ring cavity [22]. The laser itself can have hundreds to thousands of longitudinal lasing modes, all spaced at the laser free spectral range (FSR). The FSR is easy to measure by taking the laser output to a detector and measuring the beat spectrum with an electrical spectrum analyzer (ESA). Any change in test fiber temperature, T , (such as by immersing it into a thermally-controlled water bath) will result in a change in the laser FSR. Measurement of the FSR as a function of test fiber temperature reveals the fiber thermo-optic coefficient (TOC), dn/dT , from a simple calculation found in [22].

3.3 Brillouin Spectroscopy

The Brillouin gain spectrum (BGS) was measured using a heterodyne approach [23], [24]. In short, a narrow linewidth, amplified laser signal from an external cavity diode laser operating at a wavelength

TABLE 1
Some Measured and Modeled Characteristics of the Optical Fiber of This Study

Core Diameter	~ 6.0 μm *
Mode Index (@1534 nm)**	1.45247
Guided modes (@ 1534 nm)	LP ₀₁ , LP ₀₂ , LP ₁₁
Mode Area (@1534 nm)**	32.23 μm ²
Attenuation (@ 1534 nm)	20 dB/km
dn/dT***	10.72×10 ⁻⁶ K ⁻¹
Brillouin Frequency Shift, ν _B ****	11.570 GHz
dν _B /dT	0.879 MHz/K
Brillouin Spectral Width, Δν _B ****	95 MHz
Brillouin Gain g _B	0.175 ×10 ⁻¹¹ m/W

*Considering the high-index, Al-rich region.

**Calculated from the RIP.

***Measurement comes 75% uncertainty.

****Mode with the largest scattering amplitude.

of 1534 nm is launched into one end of a short (usually less than a few meters to avoid exciting stimulated Brillouin scattering) test fiber through a circulator. The Brillouin back-scattered signal is collected from the third arm of the circulator, amplified, and analyzed with a fast PIN photodiode connected to an ESA. The local oscillator signal was taken from the partial reflection from the test fiber output facet. The measured Brillouin scattering frequency is used to determine the acoustic velocity (V_a) of the glass through the relationship $V_a = \frac{\nu_a \lambda_0}{2n_m}$, where ν_a is the Brillouin frequency, λ_0 is the optical wavelength (1534 nm), and n_m is the modal refractive index, which is calculated from the RIP. In order to determine the thermal response of the Brillouin signal, same measurement was repeated with the fiber inserted into a heated water bath at several different temperatures.

The absolute Brillouin gain coefficient (BGC, or g_B) was estimated by comparing the strength of Brillouin backscatter from the test fiber with that from a fiber of known BGC [25], [26], while using the theory that is found in [27]. In the experimental configuration, a segment of the test fiber is spliced to the fiber of known BGC, necessitating careful characterization of the consequent splice loss and background loss at 1534 nm (both are nearly negligible in the present case). The mode effective area that is used for the calculation is also calculated from the RIP. A few selected fiber properties (obtained through experimental measurement or theoretical modeling) are provided in Table 1, with some becoming more relevant later in the paper.

4. Modeling

The fiber used in this study possessed the possibility of four constituents: Al₂O₃, P₂O₅, AlPO₄, and SiO₂. To model this system, a modern form of the Winkelmann-Schott [9], [28] addition model was used to calculate the bulk properties of a mixture of glass materials. The general equation governing the mixture is given by

$$G = \sum_i g_i x_i \quad (1)$$

where g is the bulk characteristic of constituent i ($i = 1, 2, 3, 4$ for a quaternary system), x is the additivity parameter (often the volume fraction in this case), and G is the property of the aggregate

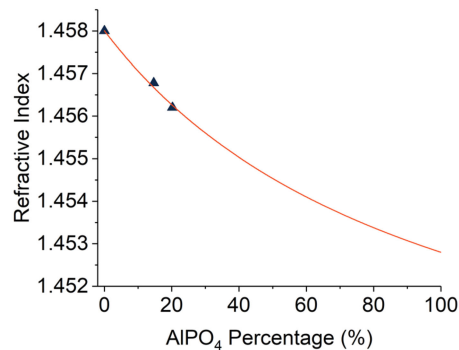


Fig. 2. Refractive index versus AlPO₄ concentration (mole %) in silica for measured data from [13] (triangles) and modeling fit (solid line).

bulk glass, such as refractive index, TOC, etc. The compositions throughout the remainder of this paper will be presented in terms of the mole % of constituent, and therefore the volume fractions can easily be calculated by knowing the molar volume of each constituent (molar mass divided by density) [29], [30]. Mass density (ρ) of a mixture has long been calculated in this manner [31].

Aside from the RIPs, the subsequent measurements on the optical fiber are modal values (either optical or acoustic modes) and, therefore, to model the material properties, a step-wise approximation to the fiber profile is assumed, with a sufficient number of layers used to ensure that the calculations converged. Each layer is taken to have a unique composition, and, as a result, unique material properties (that also may be functions of T) from which modal values can be calculated. More details on the additivity of the material index (n) can be found in [13] and the acoustic velocity in [32], both of which utilize the volume fraction as the additivity parameter, as do the TOC [22], n_2 [33], and Poisson ratio [34]. The model describing the coefficient of thermal expansion (CTE) has been modified from the form in Eqn. (1), and that model can be found in [35]. The photoelastic constants (p_{11} and p_{12}) have been found to be well-described by additivity in volume fraction, but they are carried through the refractive index via the stress and strain coefficients [34]. It should be pointed out that the doped core material often will have a CTE larger than that of a surrounding pure silica cladding, such as is the case here. As fiber temperature is increased, there is increasing pressure on the core as its thermal expansion is restricted by the much more voluminous cladding. This has a secondary influence on the core index and acoustic velocity that enters into the model as a correction [22], [36]. More details on these various models can be found summarized in [9], and the model utilized to calculate the acoustic modes can be found in [37], [38].

To use the model, the physical characteristics for the SiO₂, P₂O₅, and Al₂O₃ constituents are first assumed to be fixed to those that can be found in [39] (SiO₂ and Al₂O₃), [40] (SiO₂ Sellmeier coefficients), [33] (Al₂O₃ Sellmeier equation), and [36], [41], [42] (P₂O₅). The parameters for AlPO₄ then are used as fit parameters, adjusting them until the calculation matches the measurement. These then are taken to be the bulk characteristics of “amorphous AlPO₄.” To begin, an assumption for the mass density is required. As stated by DiGiovanni, *et al.* [13], “the two structures AlPO₄ and 2SiO₂ contain the same volume, but the AlPO₄ unit has slightly more mass.” Therefore, the mass density of AlPO₄ is taken to be that of SiO₂ (2200 kg/m³) scaled up by the ratio of the molar mass of AlPO₄ to 2SiO₂, giving 2233 kg/m³. Next, the refractive index model is fitted to the data in [13, Fig. 3] in order to achieve a benchmark refractive index value. The index values used here (from [40]) are somewhat different than those in [13], where they use a value of 1.458 at 623 nm for pure silica. Using the data from [40], this same index is obtained at 601 nm, and therefore, the values presented here will be those identified with 601 nm. Fitting the model to the data (see Fig. 2) for the binary (SiO₂-AlPO₄) glass gives a refractive index of 1.4528 for ‘fictitious’ pure, bulk, amorphous AlPO₄ at a wavelength of 601 nm. This value will be used later in the paper. It should be pointed

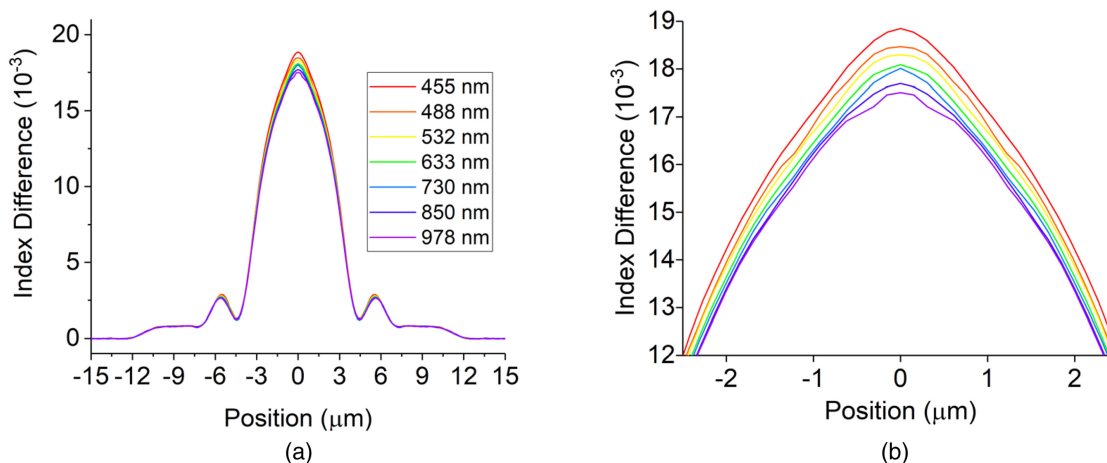


Fig. 3. (a) RIPs measured for the optical fiber at seven different wavelengths. (b) A magnified view of the peak from (a).

out that the model here is not linear across all compositions, as it is in [15]. However, it can be approximated as linear across small compositional ranges. Additionally, although the (empirical) model is not meant to suggest anything relating to the specific bonding nature of the glass, it can, as will be shown, provide meaningful qualitative insight, such as estimation of the proportion of Al₂O₃ and P₂O₅ that do not react to form AlPO₄ [20].

5. Results

5.1 Refractive Index

Fig. 3 shows the results of the multi-wavelength RIP measurements. The RIP has some structure, but the high apparent NA of the fiber clearly is dominated by the aluminum rich region in the central part of the core. It also is obvious that the outer doped region, consisting of similar molar concentrations of Al and P, has a reduced index, to just above that of silica. This region, therefore, takes on the role more so of an inner cladding structure for the fiber, rather than being part of the core. Calculations disclose that this fiber supports the LP₀₁, LP₀₂, and LP₁₁ modes at 1534 nm, making it few-moded, although operating near to cutoff at that wavelength. Additionally, two-dimensional RIPs showed that this fiber possesses slight ellipticity, mainly confined to the outer regions, beyond a radial position of about 5 μm. As a result, vertical and horizontal RIP linescans were averaged for the analysis. Finally, there is a clear reduction in the value of the index difference with increasing wavelength, as shown in the closeup in Fig. 3(b).

The compositional data shall be used for the modeling efforts, however, there are WDX data points at only a finite number of positions which do not necessarily overlap with RIP sampling positions. As a result, the RIPs were interpolated using commercial software (Wolfram Mathematica) at the positions of the WDX measurements. The set of analyses begins with the assumption that the formation of AlPO₄ was complete, meaning that all available Al₂O₃ + P₂O₅ pairs created 2AlPO₄. As part of this assumption, the balance is of the form of Al₂O₃. Using the model described above for the refractive index, and using Sellmeier coefficients for SiO₂ [40] and Al₂O₃ [33], the refractive index required of AlPO₄ to have the model match the measurement is calculated for each of 10 WDX data points between radial positions of -4.25 μm and 4.75 μm, and at each of the measurement wavelengths. The result is shown in Fig. 4(a) for the five positions for $r > 0$ (positions for $r < 0$ are left off for visual clarity). Also shown in Fig. 4(b) is the index difference between silica and AlPO₄ at each of the WDX data positions at a wavelength of 978 nm. Putting aside the uncertainty in the assumed refractive index values of either of, or both, silica and alumina, and errors in the

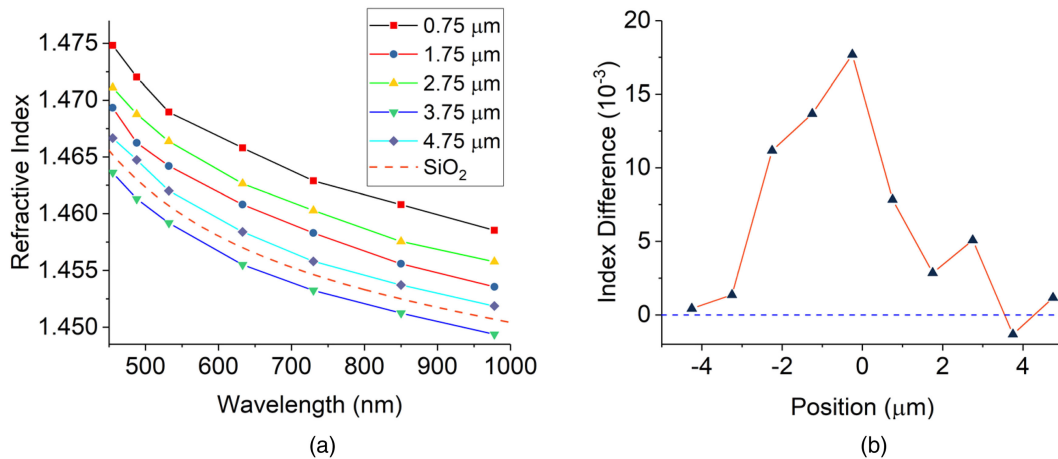


Fig. 4. (a) Refractive index versus wavelength of AlPO₄ (assuming complete formation) for each of the WDX measurement positions in the range of $r = 0.75 \mu\text{m}$ to $4.75 \mu\text{m}$. (b) Index difference between that of SiO₂ and AlPO₄ for each of the 10 WDX measurement positions at a wavelength of 978 nm.

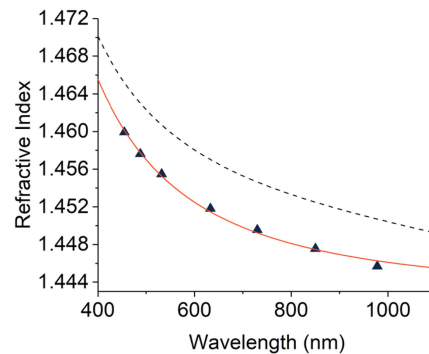


Fig. 5. Best effort chromatic dispersion curve for AlPO₄ (red solid line), obtained with the assistance of literature data [13]. For comparison, the black dashed line is the chromatic dispersion curve for SiO₂.

WDX measurements, the results clearly suggest different ratios of incomplete AlPO₄ formation at the different radial positions. Interestingly, all but one ($r = 3.75 \mu\text{m}$) of the measurements gives refractive index values above that of SiO₂ with the relative requisite AlPO₄ index increasing towards core center. As calculated and discussed further below, the core center possesses the highest percentage of phosphorus that does not form AlPO₄.

Next, the chromatic dispersion curve is approximated with the assistance of the data in [13] and the result embodied by Fig. 1. As discussed in Section 4, the AlPO₄ refractive index is 5.2×10^{-3} below that of silica at 601 nm. Given the similarity of the shapes of the SiO₂ and AlPO₄ dispersion curves (according only to Fig. 4(a) SiO₂ and the $3.75 \mu\text{m}$ position), the $r = 3.75 \mu\text{m}$ data is uniformly shifted downward (via subtraction) such that the index at 601 nm roughly matches the value 1.4528. The result of this action represents a best estimate for the chromatic dispersion curve for the AlPO₄ dopant and is shown in Fig. 5 with comparison to the chromatic dispersion curve for SiO₂. Considering the Sellmeier equation, the best fit is given by a single-oscillator (with wavelength λ in nm) as

$$n^2 = 1 + \frac{1.081051496\lambda^2}{\lambda^2 - 9310.155817} \quad (2)$$

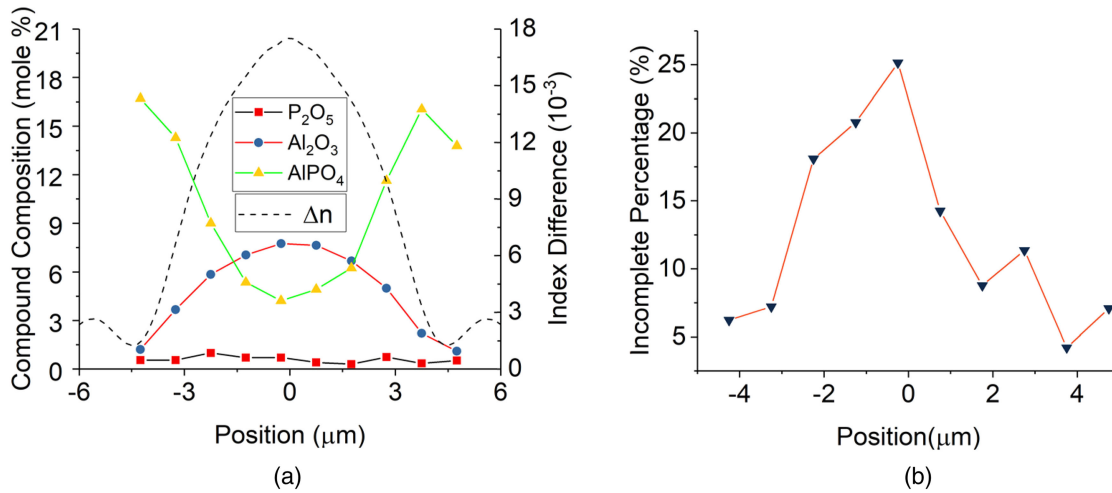


Fig. 6. (a) Compositional profile calculated using the AlPO_4 dispersion curve in Fig. 5, and previously assumed values for SiO_2 and Al_2O_3 . The refractive index (@978 nm) is provided for comparison purposes. It is found that a small fraction of elemental P forms the P_2O_5 phase. (b) Percentage of phosphorus that does not form AlPO_4 .

This result may be used with the Boling-Glass-Owyong (BGO) approximation [43] to estimate the nonlinear refractive index, n_2 . Using the expression

$$n_2 \left(10^{-13} \text{esu} \right) = 391 \frac{(n_d - 1)}{v_d^{5/4}} \quad (3)$$

where n_d is the refractive index for AlPO_4 at the wavelength of the helium d line (587.56 nm), and v_d is the Abbe number, the nonlinear index for AlPO_4 is calculated to be 0.97×10^{-13} esu (2.81×10^{-20} m^2/W at $\lambda = 1 \mu\text{m}$). Within experimental uncertainty, this is nearly identical to that of SiO_2 derived from the data in [40] (0.92×10^{-13} esu or 2.66×10^{-20} m^2/W at $\lambda = 1 \mu\text{m}$). Therefore, the addition of AlPO_4 is expected to have essentially no influence on the strength of the Kerr nonlinearities when added to silica, although this requires further experimental validation.

Next, the deduced chromatic dispersion data will be used to estimate the proportion of non-joined Al_2O_3 and P_2O_5 , resulting in excess Al_2O_3 and P_2O_5 (which serve to raise the refractive index). In this case, the same refractive index values for silica and alumina are again assumed, and the refractive index of AlPO_4 is taken to be that in Fig. 5. Then, with incomplete AlPO_4 formation, the system is assumed to be a quaternary glass comprised of constituents SiO_2 , AlPO_4 , P_2O_5 , and Al_2O_3 . The refractive index of P_2O_5 (0.044 above that of silica) is taken from [41]. Since the index in [41] was measured at $\sim 1 \mu\text{m}$, this analysis will be performed only at 978 nm. Finally, with all these details in place, the composition can be described to be (for clarity, the WDX data points analyzed here are all in alumina rich regions)

$$\alpha \cdot \text{P}_2\text{O}_5 + (\alpha + \beta) \cdot \text{Al}_2\text{O}_3 + (\gamma - 2\alpha) \text{AlPO}_4 + (100 - \beta - \gamma) \text{SiO}_2 \quad (4)$$

where α is the molar concentration of P_2O_5 that did not react to form AlPO_4 . β and γ are the Al_2O_3 and AlPO_4 concentrations, respectively, assuming complete join formation. The model then is used to determine that α which is necessary for the modeled refractive index difference to match the measured value. The result of the calculated composition of P_2O_5 , Al_2O_3 , and AlPO_4 is shown in Fig. 6(a), and the percentage of phosphorus that does not form AlPO_4 is shown in Fig. 6(b). Interestingly, in all Al-rich layers there appears to be some P_2O_5 that forms, ranging from about 0.3 to 1 mole %, and presenting a hint of azimuthal symmetry with a pair of local maxima at $r = 2.5 \mu\text{m}$. This distribution is in some contrast to the results in [20] (where more complete AlPO_4 formation

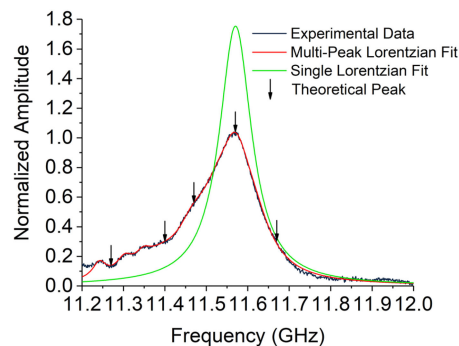


Fig. 7. Measured Brillouin signal from the optical fiber and modeling fit (red line). The green curve is a single Lorentzian function that has the same integrated intensity as the measured data from 11.2 GHz to 12 GHz. The spectrum at frequencies less than 11.2 GHz was dominated by the system response and is not shown here. The arrows indicate the position of the modes according to the model in [37].

was observed in glasses with excess Al₂O₃ or P₂O₅), however, this most likely stems from differing optical fiber processing conditions.

5.2 Thermo-Optic Coefficient

An attempt was made to calculate the CTE using the model in [35] from the data in [13]. In short, these efforts were unsuccessful. Calculations varied by over an order-of-magnitude, and therefore a reliable CTE could not be extracted from the data. Instead, a baseline estimate could be made with the assistance of data for crystalline AlPO₄, called “berlinite” [44]. Averaging the CTE across the two provided lattice constants gives $12.8 \times 10^{-6} \text{ K}^{-1}$, quite high when compared with that of pure silica.

The TOC measurement was somewhat unreliable due to difficulty in maintaining single mode operation in the fiber. Since the fiber was close to single mode, the fiber could successfully be coiled to strip the higher order modes (HOMs) from the optical fiber. However, this also introduced birefringence that resulted in polarization-related effects in the measurement. Depending on the fiber configuration, TOCs in the range of $10.3 \times 10^{-6} \text{ K}^{-1}$ to $11.5 \times 10^{-6} \text{ K}^{-1}$ were observed. A best effort was undertaken to configure the fiber so that it could offer repeatable measurements, and a few somewhat repeatable numbers in the vicinity of $10.72 \pm 0.05 \times 10^{-6} \text{ K}^{-1}$ were observed. Using this central value, and the AlPO₄ CTE presented above (CTE data for the other constituents may be found in [35]), the TOC for AlPO₄ is calculated to be $8.3 \times 10^{-6} \text{ K}^{-1}$ (or about 20% lower than that of SiO₂). However, if considering the minimum and maximum measured TOC value, the calculated TOC for AlPO₄ can vary from $5.1 \times 10^{-6} \text{ K}^{-1}$ to $14.6 \times 10^{-6} \text{ K}^{-1}$, which is around 75% uncertainty from the central value. Further work is underway to try to gain a better grasp of this value by fabrication of single-mode fibers with similar composition. There may also be further secondary influences from the distribution of CTE within the fiber. Interestingly, this value is not far from that of silica, even though P₂O₅ has a negative TOC [22], further illustrating the distinct behavior of AlPO₄.

5.3 Brillouin Spectroscopy

Fig. 7 shows the measured Brillouin spectrum with a multi-peak Lorentzian fit. While the high frequency tail of the central peak (located at 11.5704 GHz) roughly follows a Lorentzian function, several additional peaks at the low frequency side were observed, corresponding to acoustic modes residing in the inner cladding (low-index high-AlPO₄ region of the fiber). Using the acoustic velocity of pure silica and the calculated modal refractive index of the fiber at 1534 nm ($n_m = 1.45247$), the Brillouin frequency in the outer cladding is calculated to be 11.305 GHz, setting the boundary between guided and anti-guided acoustic modes in the measured spectrum. More specifically,

modes with frequencies greater than this value are acoustically anti-guided. Fitting results show that the Brillouin signals for the anti-guided modes have a full-width at half-maximum (FWHM) of 95 MHz, while the guided modes have a narrower FWHM in the vicinity of 50 MHz, indicating less loss for the guided acoustic modes. This is discussed further below.

Using the methodology summarized in Section 3.3, the fiber has an as-measured BGC of 0.175×10^{-11} m/W. However, calculation of the BGC of the material, as is required to deduce p_{12} , from such a multi-peak Brillouin signal is somewhat challenging. To do this, a single Lorentzian function with the same central frequency and FWHM as the main peak is assumed, and with an amplitude set such that its integrated intensity is the same as that of the measurement data in the wavelength range from 11.2 to 12 GHz. This way, the BGS reduces from a multi-acoustic-mode on to an effectively single-anti-guided acoustic mode, and from which material properties may be calculated. This result is shown as the green line in Fig. 7, which indicates a peak value increase of 1.689 times. Taking this into account, the single-frequency BGC is calculated to be 0.295×10^{-11} m/W.

The acoustic system is modeled using the theory that can be found in [37]. First, the core is approximated by 5 layers corresponding to the WDX measurements. In each of these layers, the quaternary glass composition then is taken to be that derived in Fig. 6, such that the acoustic properties of those layers can be calculated from these compositions. Finally, the acoustic velocity of AIPO₄ is used as a single fitting parameter that is adjusted until the calculated acoustic mode phase velocity matches that of the fiber. This final calculated acoustic velocity for AIPO₄ is 5393 m/s. Therefore, it can be concluded that AIPO₄ decreases the acoustic velocity when added to silica. The acoustic velocities used for P₂O₅ and Al₂O₃ in the modeling were 3936 m/s and 9790 m/s, respectively, so the acoustic velocity of AIPO₄ is conclusively less than the average of those two values. This value also compares well with that calculated for bulk crystalline AIPO₄ berlinite (4942 m/s) from the c_{11} elastic constant [44]. Finally, and for completeness, the acoustic mode frequency of 11.570 GHz gives an acoustic mode velocity of 6109.7 m/s, and the acoustic mode frequencies, according to modeling results, are identified in Fig. 7 with the arrows.

The model assumes an infinite cladding and therefore propagation constants are complex, thereby providing the waveguide-derived attenuation coefficients. When the acoustic mode phase velocity is greater than that of pure silica (the outer cladding), longitudinal waveguide loss can dominate, significantly broadening the spectrum [45]. When the phase velocity is lower, the acoustic mode propagates with relatively low waveguide loss, contributed to only by radial waves propagating from the core [46]. In the latter case, the BGS spectral width ($\Delta\nu_B$) is dominated by viscoelastic damping of the acoustic wave (i.e., the phonon lifetime). The fundamental mode is calculated to have a longitudinal waveguide attenuation that adds 37.9 MHz broadening to the BGS. Subtracting this from the fitted 95 MHz gives an intrinsic material-based acoustic attenuation of 57.1 MHz. Using the acoustic power overlap method outlined in [47] (see Eqn. (3)), the spectral width of AIPO₄ is fitted, again until the calculation matched the 57.1 MHz intrinsic linewidth. The result is a spectral width of 141 MHz at a reference acoustic frequency of 11 GHz, also coming in at less than the average of the P₂O₅ and Al₂O₃ values.

The next parameter to be presented here is an estimate of the Pockels photoelastic constant p_{12} . First, the measured Brillouin gain coefficient, with the assumption that the fiber is effectively single-acoustic-mode is 0.295×10^{-11} m/W. Since p_{12} is a material-related quantity, the first step is to remove the effect of acoustic anti-guidance from this value. This can simply be done by scaling using the ratio of the measured spectral width (95 MHz) to the intrinsic value (57.1 MHz) giving a value of 0.49×10^{-11} m/W. To calculate the gain, g_B for each layer of the approximation was calculated using the expression [48]

$$g_B = \frac{2\pi n^7 p_{12}^2}{c\lambda_0^2 \rho V_a \Delta\nu_B} \quad (5)$$

with the relevant quantities being those of the material comprising the layer (and $\Delta\nu_B$ calculated at the mode frequency of 11.570 GHz). p_{12} for the AIPO₄ component is the only unknown and therefore is used as a single fit parameter, looping until for the fiber $g_B = 0.49 \times 10^{-11}$ m/W is calculated.

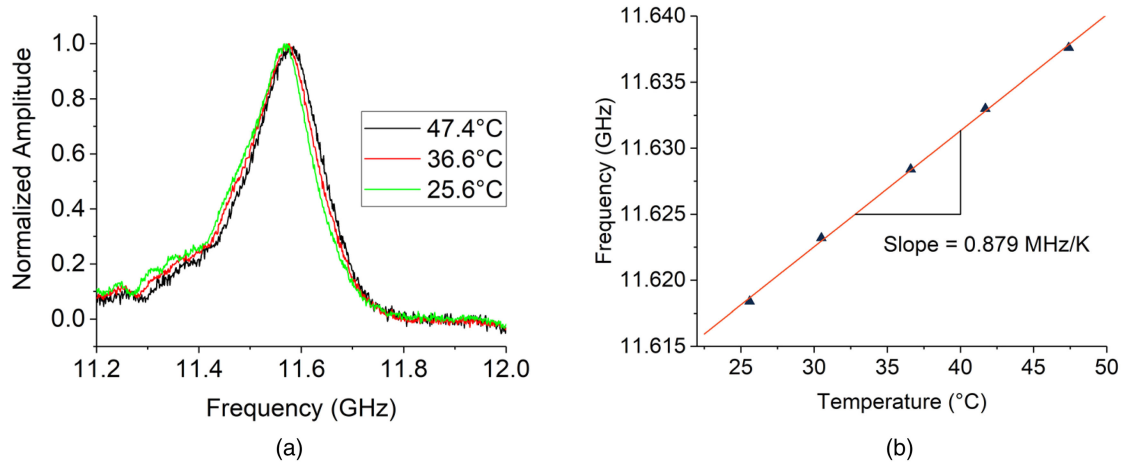


Fig. 8. (a) Brillouin signal from the optical fiber at different temperature. (b) Frequency at the normalized amplitude of 0.6 at different temperatures.

The additivity model [34] for the photoelastic constants requires knowledge of the Poisson ratio which we take to be 0.12, again with the assistance of crystalline berlinite [49], although its value was found to not influence the calculations very much. To account for the radial distribution of g_B , the following overlap calculation is performed

$$g_B(r) = \left(\int \sqrt{g_B(r)} u(r) E^2(r) r dr \right)^2 \quad (6)$$

which becomes a sum of integrals for the layered approximation, with $g_B(r)$ taking on the values for the layers, E^2 the normalized electric field power for the optical mode, and $u(r)$ is the normalized acoustic displacement vector. The integral without the g_B components is the well-known acousto-optic overlap integral for the Brillouin interaction. Since g_B is proportional to the square of the overlap integral [38], this form was selected. As it turns out, integrating with $g_B(r)$ (not its square-root) gives essentially the same result (within a few percent), as does a simple overlap integral between g_B and $u(r)$, so the basic form of the overlap that is used does not significantly impact the results. That said, using $p_{12} = 0$ for AlPO₄ gives $g_B = 0.53 \times 10^{-11}$ m/W for the quaternary glass core fiber, which is close to the target value of $g_B = 0.49 \times 10^{-11}$ m/W. So, the conclusion is that, as observed for the present fiber, p_{12} has a value around zero for AlPO₄. This result is somewhat surprising, since the other network formers, including GeO₂, P₂O₅, and B₂O₃ all have p_{12} values more similar to that of silica (a list can be found in [50]), although the result is consistent with other intermediates and modifiers including lanthana [26], alumina [51], and CaO [52]. Considering the theory that can be found in [53, eq. (19)], and using the refractive index values determined by Eqn. (2) above, AlPO₄ would need to have a nonlinear polarizability value about three times that of silica to achieve the observed result for p_{12} .

Finally, the Brillouin signals at different temperatures are measured and Fig. 8(a) is a representative example that includes several of them. To determine the thermal response of the Brillouin signal, while avoiding ambiguity in the peak frequency due to the influence of HOMs, the frequencies are first measured at the normalized amplitude of 0.6 at different temperatures. The results are shown in Fig. 8(b), with a linear fit giving a slope of 0.879 MHz/K. The same process considering normalized amplitudes of 0.5 and 0.7 gives similar results, with a variation of ± 0.04 MHz/K. Calculating the influence by AlPO₄, this gives a thermo-acoustic coefficient (TAC) in the range of -0.028 m/s/K and $+0.159$ m/s/K (0.066 m/s/K central value). This is less than that of silica, and a negative value would be consistent with results for crystalline AlPO₄ berlinite [44] where the elastic constant c_{11} is found to decrease with increasing temperature. This calculation considered the TOC but did not consider

pressure induced changes to the acoustic velocity [36], since many previous works by these authors have been similarly presented. By way of comparison, the addition of AlPO₄ to silica decreases the thermal response of Brillouin scattering much less than the addition of alumina.

6. Conclusions

A silica clad optical fiber with a core possessing SiO₂, P₂O₅, Al₂O₃, and AlPO₄ was investigated in order to enumerate a wider range of effects of AlPO₄ on the optical and acoustic properties when added to silica. Modeling this quaternary system was accomplished via a relatively simple additive approach. First, multi-wavelength RIP measurements were provided at different radial positions on the fiber, with the goal of establishing a best estimate for the bulk, glassy AlPO₄ chromatic dispersion curve. Using the BGO approximation, AlPO₄ is found to have a value of n_2 that is about 6% higher than that of silica at a wavelength of 1 μm . It is therefore expected to have little or no impact on the Kerr nonlinearities. Its thermo-optic coefficient was estimated to be $8.3 \times 10^{-6} \text{ K}^{-1}$, but this data comes with 75% uncertainty and a single-mode version of this fiber will be fabricated to better characterize the TOC. The chromatic dispersion curve then was used with the measured refractive index data to conclude that an average of about 0.5 mole% P₂O₅ exists in Al-rich regions of the fiber core, suggesting incomplete AlPO₄ formation.

With regard to the acoustic properties, AlPO₄ is found to contribute an acoustic velocity of 5393 m/s to the glass system, provide increased viscoelastic damping thereby broadening the Brillouin gain spectrum, and decrease the strength of the dependence of Brillouin scattering frequency on fiber temperature. The acousto-optic interaction is weakened through its reduction of p_{12} when added to silica. Somewhat surprisingly, and inconsistent with other network formers, the data suggests a near-zero p_{12} , consistent instead with some network modifiers and intermediates.

References

- [1] J. Dawson *et al.*, "Analysis of the scalability of diffraction-limited fiber lasers and amplifiers to high average power," *Opt. Exp.*, vol. 16, no. 17, pp. 13240–13266, 2008.
- [2] D. Richardson, J. Nilsson, and W. Clarkson, "High power fiber lasers: Current status and future perspectives," *J. Opt. Soc. Amer. B*, vol. 27, no. 11, pp. B63–B92, 2010.
- [3] P. Zhou, X. Wang, Y. Ma, H. Lü, and Z. Liu, "Review on recent progress on mid-infrared fiber lasers," *Laser Phys.*, vol. 22, no. 11, pp. 1744–1751, 2012.
- [4] C. Jauregui, J. Limpert, and A. Tünnermann, "High-power fibre lasers," *Nature Photon.*, vol. 7, pp. 861–867, 2013.
- [5] M. Fermann and I. Hartl, "Ultrafast fibre lasers," *Nature Photon.*, vol. 7, pp. 868–874, 2013.
- [6] M. Zervas, "High power ytterbium-doped fiber lasers—Fundamentals and applications," *Int. J. Modern Phys. B*, vol. 28, no. 12, 2014, Art. no. 1442009.
- [7] M. Zervas and C. Codemard, "High power fiber lasers: A review," vol. 20, no. 5, 2014, Art. no. 0904123.
- [8] S. Fu *et al.*, "Review of recent progress on single-frequency fiber lasers," *J. Opt. Soc. Amer. B*, vol. 34, no. 3, pp. A49–A62, 2017.
- [9] P. Dragic, M. Cavillon, and J. Ballato, "Materials for optical fiber lasers: A review," *Appl. Phys. Rev.*, vol. 5, no. 4, 2018, Art. no. 041301.
- [10] D. Jain, Y. Jung, P. Barua, S. Alam, and J. Sahu, "Demonstration of ultra-low NA rare-earth doped step index fiber for applications in high power fiber lasers," *Opt. Exp.*, vol. 23, no. 6, pp. 7407–7415, 2015.
- [11] P. Laperle, C. Paré, H. Zheng, A. Croteau, and Y. Taillon, "Yb-doped LMA triple-clad fiber laser," *Proc. SPIE*, vol. 6343, 2006, Art. no. 63430X.
- [12] L. Dong, "Advanced optical fibers for high power fiber lasers," in *Advances in Optical Fiber Technology: Fundamental Optical Phenomena and Applications*, M. Yasin, Ed. London, U.K.: InTech, 2015, ch. 7, pp. 221–252.
- [13] D. DiGiovanni, J. MacChesney, and T. Kometani, "Structure and properties of silica containing aluminum and phosphorus near the AlPO₄ join," *J. Non-Crystalline Solids*, vol. 113, pp. 58–64, 1989.
- [14] G. Vienne *et al.*, "Role of aluminum in Ytterbium-Erbium codoped phosphoaluminosilicate optical fibers," *Opt. Fiber Technol.*, vol. 2, no. 4, pp. 387–393, 1996.
- [15] S. Unger, A. Schwuchow, J. Dellith, and J. Kirchhof, "Codoped materials for high power fiber lasers—Diffusion behaviour and optical properties," *Proc. SPIE*, vol. 6469, 2007, Art. no. 646913.
- [16] M. Likhachev, M. Bubnov, K. Zotov, D. Lipatov, M. Yashkov, and A. Guryanov, "Effect of the AlPO₄ join on the pump-to-signal conversion efficiency in heavily Er-doped fibers," *Opt. Lett.*, vol. 34, no. 21, pp. 3355–3357, 2009.
- [17] S. Jetschke, S. Unger, A. Schwuchow, M. Leich, and J. Kirchhof, "Efficient Yb laser fibers with low photodarkening by optimization of the core composition," *Opt. Exp.*, vol. 16, no. 20, pp. 15540–15545, 2008.
- [18] J. Koponen, M. Söderlund, S. Tammela, and H. Po, "Photodarkening in ytterbium-doped silica fibers," *Proc. SPIE*, vol. 5990, 2005, Art. no. 599008.

- [19] T. Deschamps, H. Vezin, C. Gonnet, and N. Ollier, "Evidence of AIOHC responsible for the radiation-induced darkening in Yb doped fiber," *Opt. Exp.*, vol. 21, no. 7, pp. 8382–8392, 2013.
- [20] S. Kuhn *et al.*, "Modelling and the refractive index behavior of Al,P-doped SiO₂, fabricated by means of all-solution doping, in the vicinity of Al:P = 1:1," *Opt. Mater. Exp.*, vol. 8, no. 5, pp. 1328–1340, 2018.
- [21] A. Yablon, "Multi-wavelength optical fiber refractive index profiling by spatially resolved Fourier transform spectroscopy," *J. Lightw. Technol.*, vol. 28, no. 4, pp. 360–364, Feb. 2010.
- [22] P. Dragic, M. Cavillon, and J. Ballato, "On the thermo-optic coefficient of P₂O₅ in SiO₂," *Opt. Mater. Exp.*, vol. 7, no. 10, pp. 3564–3661, 2017.
- [23] P. Dragic, "Brillouin spectroscopy of Nd-Ge co-doped silica fibers," *J. Non-Crystalline Fibers*, vol. 355, pp. 403–413, 2009.
- [24] P. Dragic, P. Law, J. Ballato, T. Hawkins, and P. Foy, "Brillouin spectroscopy of YAG-derived optical fibers," *Opt. Exp.*, vol. 18, no. 10, pp. 10055–10067, 2010.
- [25] P. Dragic *et al.*, "Athermal distributed Brillouin sensors utilizing all-glass optical fibers fabricated from rare earth garnets: LuAG," *New J. Phys.*, vol. 18, 2016, Art. no. 105004.
- [26] P. Dragic, C. Kucera, J. Ballato, D. Litzkendorf, J. Dellith, and K. Schuster, "Brillouin scattering properties of lanthano-aluminosilicate optical fiber," *Appl. Opt.*, vol. 53, no. 25, pp. 5660–5671, 2014.
- [27] R. Boyd, K. Rzaewski, and P. Narum, "Noise initiation of stimulated Brillouin scattering," *Phys. Rev. A*, vol. 42, 1990, Art. no. 5514.
- [28] A. Winkelmann and O. Schott, "On the elasticity and the tensile and compressive strength of several new glasses in their dependence on the chemical composition," *Ann. Phys. Chem.*, vol. 51, pp. 697–730, 1894.
- [29] P. Dragic, "Simplified model for effect of Ge doping on silica fibre acoustic properties," *Electron. Lett.*, vol. 45, pp. 256–257, 2009.
- [30] P. Dragic, "Brillouin gain reduction via B₂O₃ doping," *J. Lightw. Technol.*, vol. 29, no. 7, pp. 967–973, Apr. 2011.
- [31] F. Bloss, "Relationship between density and composition in mol per cent for some solid solution series," *Amer. Mineralogist*, vol. 37, no. 11/12, pp. 966–981, 1952.
- [32] P. Dragic, "The acoustic velocity of Ge-doped silica fibers: A comparison of two models," *Int. J. Appl. Glass Sci.*, vol. 1, no. 3, pp. 330–337, 2010.
- [33] P. Dragic, M. Cavillon, and J. Ballato, "The linear and nonlinear refractive index of amorphous Al₂O₃ deduced from aluminosilicate optical fibers," *Int. J. Appl. Glass Sci.*, vol. 9, no. 3, pp. 421–427, 2018.
- [34] C. Ryan, J. Furtick, C. Kucera, R. Stolen, J. Ballato, and P. Dragic, "Pockels coefficients in multicomponent oxide glasses," *Int. J. Appl. Glass Sci.*, vol. 6, no. 4, pp. 387–396, 2015.
- [35] M. Cavillon, P. Dragic, and J. Ballato, "Additivity of the coefficient of thermal expansion in silica optical fibers," *Opt. Lett.*, vol. 42, no. 18, pp. 3650–3653, 2017.
- [36] P. Dragic, S. Martin, A. Ballato, and J. Ballato, "On the anomalously strong dependence of the acoustic velocity of alumina on temperature in aluminosilicate glass optical fibers—Part I: Material modeling and experimental validation," *Int. J. Appl. Glass Sci.*, vol. 7, no. 1, pp. 3–10, 2016.
- [37] P. Dragic, "Novel dual-Brillouin-frequency optical fiber for distributed temperature sensing," *Proc. SPIE*, vol. 7197, 2009, Art. no. 719710.
- [38] P. Dragic and J. Ballato, "A brief review of specialty optical fibers for Brillouin-scattering-based distributed sensors," *Appl. Sci.*, vol. 10, no. 8, 2018, Art. no. 1996.
- [39] M. Cavillon *et al.*, "Brillouin properties of a novel strontium aluminosilicate glass optical fiber," *J. Lightw. Technol.*, vol. 34, no. 6, pp. 1435–1441, Mar. 2016.
- [40] J. Fleming, "Dispersion in GeO₂-SiO₂ glasses," *Appl. Opt.*, vol. 23, no. 24, pp. 1486–1493, 1984.
- [41] P. Law, Y. Liu, A. Croteau, and P. Dragic, "Acoustic coefficients of P₂O₅-doped silica fiber: Acoustic velocity, acoustic attenuation, and thermo-acoustic coefficient," *Opt. Mater. Exp.*, vol. 1, no. 4, pp. 686–699, 2011.
- [42] P. Law, A. Croteau, and P. Dragic, "Acoustic coefficients of P₂O₅-doped silica fiber: The strain-optic and strain-acoustic coefficients," *Opt. Mater. Exp.*, vol. 2, no. 4, pp. 391–404, 2012.
- [43] N. Boling, A. Glass, and A. Owyong, "Empirical relationships for predicting nonlinear refractive index changes in optical solids," *IEEE J. Quantum Electron.*, vol. QE-14, no. 8, pp. 601–608, Aug. 1978.
- [44] Z. Chang and G. Barsch, "Elastic constants and thermal expansion of berlinite," *IEEE Trans. Sonics Ultrason.*, vol. SU-23, no. 2, pp. 127–135, Mar. 1976.
- [45] P. Dragic, "Brillouin suppression by fiber design," in *Proc. IEEE Photon. Soc. Summer Topicals Meeting*, 2010, Paper TuC3.2.
- [46] C. Jen, A. Safaai-Jazi, and G. Farnell, "Leaky modes in weakly guiding fiber acoustic waveguides," *IEEE Trans. Ultrason., Ferroelect., Freq. Control*, vol. UFFC-33, no. 6, pp. 634–643, Nov. 1986.
- [47] P. Dragic, C. Kucera, J. Furtick, J. Guerrier, T. Hawkins, and J. Ballato, "Brillouin spectroscopy of a novel baria-doped silica glass optical fiber," *Opt. Exp.*, vol. 21, no. 9, pp. 10924–10941, 2013.
- [48] G. P. Agrawal, "Stimulated Brillouin scattering," in *Nonlinear Fiber Optics*, 2nd ed. Orlando, FL, USA: Academic, 1995, ch. 9.
- [49] S. Ji *et al.*, "Poisson's ratio and auxetic properties of natural rocks," *J. Geophys. Res.: Solid Earth*, vol. 123, pp. 1161–1185, 2018.
- [50] P. Dragic, M. Cavillon, A. Ballato, and J. Ballato, "A unified materials approach to mitigating optical nonlinearities in optical fiber. II. B. The optical fiber, material additivity and the nonlinear coefficients," *Int. J. Appl. Glass Sci.*, vol. 9, no. 3, pp. 307–318, 2018.
- [51] P. Dragic, J. Ballato, S. Morris, and T. Hawkins, "Pockels' coefficients of alumina in aluminosilicate optical fiber," *J. Opt. Soc. Amer. B*, vol. 30, no. 2, pp. 244–250, 2013.
- [52] M. Cavillon, P. Dragic, C. Kucera, T. Hawkins, and J. Ballato, "Calcium silicate and fluorosilicate optical fibers for high energy laser applications," *Opt. Mater. Exp.*, vol. 9, no. 5, pp. 2147–2158, 2019.
- [53] N. Borrelli and R. Miller, "Determination of the individual strain-optic coefficients by an ultrasonic technique," *Appl. Opt.*, vol. 7, no. 5, pp. 745–750, 1968.